

## Numerical study of flow in a rotor-stator system with inward throughflow

M. FARZANEH-GORD<sup>1)</sup>, A. VAZIFEDOOST<sup>1)</sup>,  
A. B. KHOSHNEVIS<sup>2)</sup>

<sup>1)</sup> *The Faculty of Mechanical Engineering  
Shahrood University of Technology  
Shahrood, Iran  
e-mail: mahmood.farzaneh@yahoo.co.uk*

<sup>2)</sup> *Faculty of Engineering  
Sabzevar Tarbiat Moallem University  
Sabzevar, Iran*

A NUMERICAL STUDY has been carried out to study fluid flow within a rotor-stator system with an inward throughflow and pre-rotation. Furthermore, the effect of flow parameters on the flow structure has been investigated. The entrainment coefficient,  $\beta$ , of the rotating fluid and the rotating disc moment coefficient have been calculated. A correlation has been found for predicting the place of stagnation point. The results show the Batchelor type of flow with two separated boundary layers on the rotating and stationary discs. The numerical results are compared with the available measured data and generally, a good agreement has been encountered.

**Key words:** rotor-stator system, Batchelor-type flow, turbulent boundary layer, numerical modelling.

Copyright © 2010 by IPPT PAN

### Notations

$C_m$	moment coefficient,
$C_w = \dot{m}/\mu R_2$	non-dimensional mass flow rate,
$D, E, F$	terms appearing in the turbulent modelling,
$G = h/R_2$	aspect ratio,
$f_\mu$	wall damping function, appearing in the turbulence modelling,
$\dot{m}$	throughout mass flow rate,
$P$	rate of production of turbulent kinetic energy,
$Re_\varphi = \Omega R_2^2/\nu$	rotational Reynolds number,
$Re_h = \Omega h^2/\nu$	axial distance Reynolds number,
$R_t = \rho\kappa^2/\mu\varepsilon$	local turbulence Reynolds number,
$R_1$	outer radius of the rotor,
$R_2$	outer radius of the system,
$R_3$	inner radius of the rotor,
$R_4$	inner radius of the stator,
$S$	source terms,

$r, \phi, z$	radial, circumferential and axial coordinate system,
$V_r, V_\phi, V_z$	radial, circumferential, axial velocity component,
$v_r^* (= V_r/\Omega r)$	non-dimensional radial velocity,
$x = r/R_2$	non-dimensional radial coordinate,
$x^*$	stagnation point,
$y$	distance normal to the wall,
$y^+$	non-dimensional wall distance,
$y_{\min}$	the minimum distance between the wall and the mesh point,
$z^*$	non-dimensional axial coordinate,
$\Phi$	generalized dependent variable in transport equation,
$\rho$	density,
$\nu$	kinematic viscosity,
$\mu, \mu_t, \mu_{\text{eff}}$	dynamic, turbulent and effective viscosity,
$\beta = V_\phi/\Omega r$	entrainment coefficient,
$\Omega$	angular velocity of rotor,
$\lambda_T = C_w/\text{Re}_\varphi^{0.8}$	turbulent flow parameter,
$\Gamma_r, \Gamma_\phi, \Gamma_z$	effective diffusivities for the radial, circumferential and axial directions,
$\kappa$	turbulent kinetic energy,
$\varepsilon$	rate of dissipation of turbulent kinetic energy,
$C_\mu, C_{\varepsilon 1}, C_{\varepsilon 2}$	terms appearing in the turbulent modelling,
$f_1, f_\mu, \sigma_k, \sigma_\varepsilon$	terms appearing in the turbulent modelling,
$\tau_w$	average wall shear stress.

### Subscripts

$\infty$	far from the discs (here in the middle of the axial distance between the rotor and the stator),
$\Phi$	represents the generalised variable,

## 1. Introduction

THE FLUID FLOW within a rotor-stator system has been widely studied and was found to have many applications, especially in turbo-machinery. Moreover, it is a classical example of rotating flow in which exact solution of Navier-Stokes equation can be found.

Figure 1 shows a schematic diagram of a rotor-stator system. The system comprises two discs: one disc (the rotor) rotates with angular velocity  $\Omega$ , and the other one (the stator) is stationary. There is an axial distance,  $h$ , between the two discs.

BATCHELOR [1] has assumed that there is a boundary layer on each disc and that a rotating core is established between them, with the magnitude of the core rotation being between 0 and  $\Omega$ . The flow on the rotor is analogous to a rotating disc in a quiescent fluid, with a radial outflow of fluid entrained from the core; the flow on the stator is analogous to a rotating fluid near a stationary disc, with radial inflow of fluid and an efflux from the boundary layer to the core. STEWARTSON [19] proposed another model, suggesting that there is a boundary layer on the rotor (analogous to the von Kármán flow on the free disc), in which

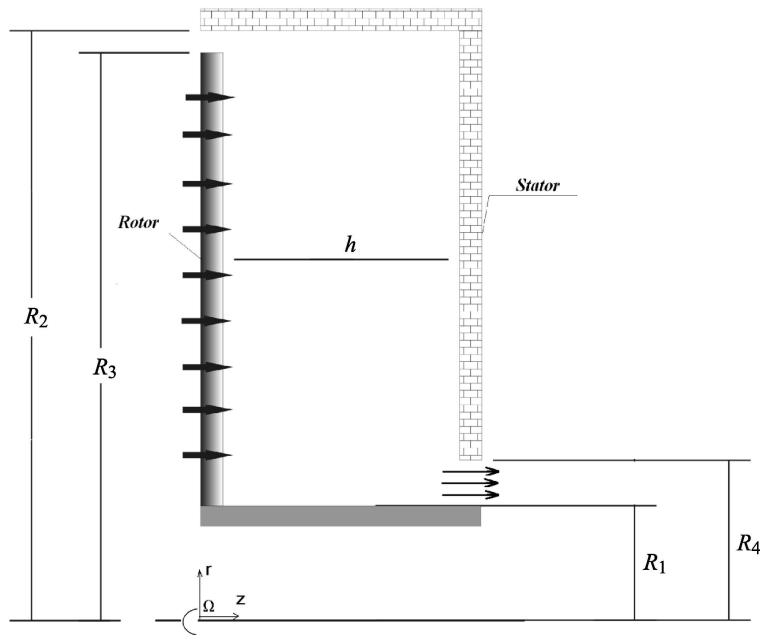


FIG. 1. A schematic diagram of the rotor-stator system.

the tangential component of velocity reduces from  $\Omega r$  on the disc to zero far from it. In this model there is no boundary layer on the stator. GROHNE [7] solved the von Kármán equations for Reynolds numbers up to  $Re_h = \Omega h^2/\nu = 100$  and found that when  $Re_h = 10$ , no core rotation was apparent, but when  $Re_h = 100$ , there was evidence of separate boundary layers and a rotating core. PÍCHA and ECKERT [17], who made the velocity measurements, found that when the discs were open to the atmosphere, no significant core rotation occurred. However, when the discs were surrounded by a stationary casing (or shroud), a core rotation did exist.

Many researchers have performed theoretical and experimental work for the rotor-stator problem. Some of them, such as LANCE and ROGERS [10], found the Batchelor-type flow, with a rotating core of fluid, and others, such as PEARSON [16], verified the Stewartson-type flow, with no rotating core. It is now known that both flow structures exist and that conditions at the edges of finite discs can affect the type of flow which occurs.

For a Batchelor-type flow, the flow structure consists of two boundary layers and a rotating core. The rotating core is defined by a tangential velocity far from the discs (mostly in the middle of axial distance), equal to  $\beta_\infty \Omega r = V_\theta$ , and a quasi-zero radial velocity: the core. The first boundary layer developed on the fixed disc; it is called the Bodewadt layer. In this layer, the tangential velocity varies between  $\beta_\infty \Omega r$  in the core to zero on the stationary disc. The

second boundary layer developed on the rotor: it is the von Kármán or Ekman layer. In this layer, the tangential velocity varies from  $\Omega r$  on the rotating disc to that of the core,  $\beta_\infty \Omega r$ . For a sealed rotor-stator system, however, a Batchelor-type flow usually occurs providing the value of  $Re_h$  to be sufficiently high to ensure separate boundary layers.

Many computational and experimental studies have been carried out to investigate the characteristics of turbulent flow and heat transfer in rotor-stator systems. WILSON *et al.* [20] summarised the work which showed that the flow and heat transfer in systems with a superposed radial outflow can be computed with reasonable accuracy using  $\kappa - \varepsilon$  turbulence models.

KARABAY *et al.* [8] has studied flow structure inside a cover plate-rotor stator system and found that the most important parameters affecting the flow structure were the inlet pre-swirl ratio, the ratio of the tangential component of velocity of the pre-swirl air to the speed of the rotating disc at the same radius, and the turbulent flow parameter  $\lambda_T = C_w / Re_\varphi^{0.8}$ , where  $C_w = \dot{m} / \mu R_2$  is the non-dimensional flow rate of the pre-swirl air and  $Re_\varphi = \Omega R_2^2 / \nu$  is the rotational Reynolds number for the disc.

FARZANEH [3] carried out measurements and three-dimensional computations for the flow structure in an idealised pre-swirl rotor-stator system and FARZANEH [4] made an axisymmetric computation. The results obtained show that the flow in the pre-swirl system has some similarities to that found in classical rotor-stator systems. The measurements and computations showed that significant losses in total pressure occurred between the inlet nozzles and the mid-axial plane between the rotor and stator (where pitot-tube measurements were made). These mixing losses, which were caused by a momentum exchange between the primary pre-swirl flow and the recirculation secondary flow, increased as the inlet pre-swirl ratio increased. LEWIS *et al.* [11] investigated the effect of the radial location of the inlet nozzles on the performance of the same system. A commercial code is used to solve the Reynolds-averaged Navier–Stokes equations using a high Reynolds number  $\kappa - \varepsilon / \kappa - \omega$  turbulence model with wall functions. They suggested that for an optimum pre-swirl configuration, an engine designer should place the pre-swirl nozzles at a high radius.

FARZANEH [5] investigated heat transfer over a rotating disc of the idealised pre-swirl rotor-stator system using a 3D steady, incompressible turbulent flow solver in a rotating frame of reference. The computed as well as the measured local heat transfer coefficients (by LOCK *et al.* [13]) show axisymmetric distribution on the rotor, except near the receiver cooling holes in which a small region of high heat transfer is observable. LEWIS *et al.* [11] compared the heat transfer measurements from a pre-swirl rotor–stator experiment with three-dimensional (3D) steady-state results from a commercial computational fluid dynamics (CFD) code. They have obtained the same results as FARZANEH [5].

PONCET *et al.* [18] have studied the behaviour of the entrainment coefficient of the turbulent flow in a rotor–stator system with throughflow, as a function of the rotational Reynolds number, of the throughflow (non-dimensional flow) rate and of the aspect ratio,  $G = h/R_2$ , of the system. In particular, they determined an analytical law, which enables to calculate the entrainment coefficient versus the local flow rate coefficient. This law has been determined analytically and has been validated by extensive pressure and velocity measurements, for different values of the axial gap and in a large range of Reynolds numbers and flow rates. They have also determined the structure of the rotating-disc flow when an inward flux was added. They concluded that, for a weak throughflow, the flow at the periphery has the same properties as in the case without flux. The Ekman boundary is centrifugal and the Bodewadt boundary layer is centripetal. These layers are separated by a central rotating core. But, for a strong throughflow, the flow in the Ekman boundary layer becomes centripetal and the core rotates faster than the rotating disc.

A rotor-stator system, as shown in Fig. 1, provides a simplified model of the flow which has been studied in this paper. It consists of a cylindrical cavity enclosed by a stationary disc (the stator) and a smooth rotating disc (the rotor). A fixed shroud surrounds the cavity.

This paper describes the effects of flow parameters such as the Reynolds number, non-dimensional flow rate and aspect ratio of the flow structure inside the system, using a computational method. The available measured data of PONCET *et al.* [18] are also compared with computed values for validating purposes.

## 2. Governing equations

The three-dimensional, steady-state, incompressible Reynolds-averaged flow equations in a cylindrical polar coordinate system  $r, \phi, z$  with velocity components  $V_r, V_\phi, V_z$  can be written in a common form:

$$(2.1) \quad \frac{1}{r} \frac{\partial}{\partial r} (\rho r V_r \Phi) + \frac{1}{r} \frac{\partial}{\partial \phi} (\rho V_\phi \Phi) + \frac{\partial}{\partial z} (\rho V_z \Phi) \\ = \frac{1}{r} \frac{\partial}{\partial r} \left( r \Gamma_r \frac{\partial \Phi}{\partial r} \right) + \frac{1}{r^2} \frac{\partial}{\partial \phi} \left( \Gamma_\phi \frac{\partial \Phi}{\partial \phi} \right) + \frac{\partial}{\partial z} \left( \Gamma_z \frac{\partial \Phi}{\partial z} \right) + S_\Phi,$$

where  $\Phi$  represents the generalised momentum variable and the net source  $S_\Phi$  is different for each component of momentum.  $\Gamma_r, \Gamma_\phi$  and  $\Gamma_z$  are the effective diffusivities for the radial, circumferential and axial directions, comprising both the laminar and turbulent components.

In this paper, turbulent flow computations have been made using the low-Reynolds number  $\kappa - \varepsilon$  turbulence models proposed by LAUNDER-SHARMA [9].

The  $\kappa - \varepsilon$  turbulence model equations can be represented in the same common form of Eq. (2.1). The relevant expressions are given in Table 1, in which  $\mu_{\text{eff}} = \mu + \mu_t$  is the effective viscosity.

**Table 1. Terms appearing in the turbulence model.**

Term	Lauder and Sharma-Morse model
$C_\mu$	0.09
$C_{\varepsilon 1}$	1.44
$C_{\varepsilon 2}$	$1.92f_1$
$D$	$2\mu \left[ \left( \frac{\partial \sqrt{k}}{\partial z} \right)^2 + \left( \frac{\partial \sqrt{k}}{\partial r} \right)^2 + \left( \frac{\partial \sqrt{k}}{r \partial \phi} \right)^2 \right]$
$E$	$2 \frac{\mu \mu_t}{\rho} \left[ \left( \frac{\partial^2 V_r}{\partial z^2} \right)^2 + \left( \frac{\partial^2 V_\phi}{\partial z^2} \right)^2 + \left( \frac{\partial^2 V_z}{\partial r^2} \right)^2 + \left( \frac{\partial^2 V_\phi}{\partial r^2} \right)^2 + \left( \frac{1}{r^2} \frac{\partial^2 V_r}{\partial \phi^2} \right)^2 + \left( \frac{1}{r^2} \frac{\partial^2 V_z}{\partial \phi^2} \right)^2 \right]$
$F$	0
$f_1$	$1 - 0.3 \exp(-R_t^2)$
$f_\mu$	$\exp \left[ 3.4 / \left( 1 + \frac{R_t}{50} \right)^2 \right]$
$\sigma_k$	1
$\sigma_\varepsilon$	1.3

In the  $\kappa - \varepsilon$  equations,  $P$  denotes the rate of production of turbulent kinetic energy and is given as follows:

$$(2.2) \quad P = \mu_t \left[ 2 \left( \left( \frac{\partial V_z}{\partial z} \right)^2 + \left( \frac{\partial V_\phi}{r \partial \phi} + \frac{V_r}{r} \right)^2 + \left( \frac{\partial V_r}{\partial r} \right)^2 \right) + \left( \frac{\partial V_z}{\partial r} + \frac{\partial V_r}{\partial z} \right)^2 + \left( \frac{\partial V_\phi}{\partial z} + \frac{V_z}{r \partial \phi} \right)^2 + \left( r \frac{\partial}{\partial r} \left( \frac{V_\phi}{r} \right) + \frac{\partial V_r}{r \partial \phi} \right)^2 \right].$$

Other terms appearing in the  $\kappa - \varepsilon$  equations are given in Table 2.  $f_\mu$  is a wall damping function associated with low Reynolds number models.  $R_t$  is a local turbulence Reynolds number and  $y^+$  is the non-dimensional distance from the solid surface:

$$(2.3) \quad R_t = \frac{\rho \kappa^2}{\mu \varepsilon}$$

and

$$(2.4) \quad y^+ = y_{\min} \frac{\sqrt{\tau_w / \rho}}{\nu}.$$

**Table 2. Components of the transport equations.**

$\phi$	$\Gamma_z$	$\Gamma_r$	$\Gamma_\phi$	$s_\phi$
1	0	0	0	0
$V_r$	$2\mu_t + \mu$	$\mu_t + \mu$	$\mu_t + \mu$	$-\frac{\partial p}{\partial v} + \frac{\rho V_\phi^2}{r} - \frac{2\mu_{\text{eff}}}{r^2} \frac{\partial V_\phi}{\partial \phi} - (2\mu_t + \mu) \frac{V_r}{r^2} - \frac{\partial(\rho k)}{\partial r}$ $+ \frac{\partial}{\partial z} \left( \mu_t \frac{\partial V_z}{\partial r} \right) + \mu_t \frac{\partial}{\partial \phi} \left( \frac{\partial}{\partial r} \left( \frac{V_\phi}{r} \right) \right)$
$V_\phi$	$\mu_t + \mu$	$2\mu_t + \mu$	$\mu_t + \mu$	$\frac{1}{r} \frac{\partial}{\partial r} \left( \mu_t \frac{\partial V_r}{\partial \phi} \right) - \frac{V_\phi}{r} \frac{\partial \mu_t}{\partial r} + \frac{3\mu_t + 2\mu}{r^2} \frac{\partial V_r}{\partial \phi} + \frac{2V_r}{r^2} \frac{\partial \mu_t}{\partial \phi}$ $- \frac{1}{r} \frac{\partial}{\partial \phi} \left( P + \rho k \right) - \frac{\mu_{\text{eff}} V_\phi}{r^2} + \frac{1}{r} \frac{\partial}{\partial z} \left( \mu_t \frac{\partial V_z}{\partial \phi} \right) - \frac{\rho V_r V_\phi}{r}$
$V_z$	$2\mu_t + \mu$	$\mu_t + \mu$	$\mu_t + \mu$	$-\frac{\partial}{\partial z} (P + \rho k) + \frac{1}{r} \frac{\partial}{\partial r} \left( r \mu_t \frac{\partial V_r}{\partial z} \right) + \frac{1}{r} \frac{\partial}{\partial \phi} \left( \mu_t \frac{\partial V_\phi}{\partial z} \right)$
$k$	$\mu + \frac{\mu_t}{\sigma_k}$	$\mu + \frac{\mu_t}{\sigma_k}$	$\mu + \frac{\mu_t}{\sigma_k}$	$P - \rho \varepsilon - D$
$\varepsilon$	$\mu + \frac{\mu_t}{\sigma_\varepsilon}$	$\mu + \frac{\mu_t}{\sigma_\varepsilon}$	$\mu + \frac{\mu_t}{\sigma_\varepsilon}$	$\frac{\varepsilon}{k} (C_{\varepsilon 1} P - C_{\varepsilon 2} \rho \varepsilon) + E$

In Eq. (2.4),  $y_{\min}$  is taken as the minimum distance between the wall and the mesh point, and  $\tau_w$  is the average wall shear stress.

### 3. Numerical method

#### Computational procedure

The governing equations were discretized using the finite-volume method with hybrid-differentiation of the convection term. The SIMPLE pressure-correction scheme is adopted within a staggered grid arrangement. The discretized equations were solved using the tri-diagonal matrix algorithm, TDMA. For improving convergence performance, a Gosman damping factor [6] was used. Yap empirical correction [14] is added to the source term of  $\varepsilon$  equation, intending to reduce unrealistically large levels of near-wall turbulence that are returned by the Launder–Sharma model in regions of flow separations.

#### Boundary conditions

No-slip boundary condition was used for the velocity components on the solid surfaces. The uniform axial velocity was used of the specified mass flow rate and the tangential velocity component was set up to have a pre-rotation flow at the inlet. At the outlet, the uniform axial velocity was used to en-

**Table 3. The boundary condition used in the computation.**

Region	$\varepsilon$	k	$V_z$	$V_\phi$	$V_r$
$z = 0, R_1 < r < R_2$	$\frac{\rho \times \kappa^{1.5}}{h}$	$\frac{V_z^2}{10^3}$	$\frac{\dot{m}}{\pi(R_2^2 - R_1^2)}$	$r\Omega$	0
$z = h, R_1 < r < R_4$	$\frac{\partial \varepsilon}{\partial r} = 0$	$\frac{\partial k}{\partial r} = 0$	$\frac{\dot{m}}{\pi(R_4^2 - R_1^2)}$	0	0
$z = h, R_4 < r < R_3$	0	0	0	0	0
$r = R_1, 0 < z < h$	0	0	0	$R_1\Omega$	0
$r = R_2, 0 < z < h$	0	0	0	0	0

sure continuity, and tangential velocities were computed from a zero normal derivative condition. The radial velocity component was set to zero at the inlet and outlet. Table 3 shows the detailed boundary conditions. It is interesting to note that the curious boundary condition has been applied for  $\kappa$ ,  $\varepsilon$  on the rotor surface. As the rotor is assumed to be porous and is the only inlet boundary, it is treated as the inlet boundary for  $\kappa$ ,  $\varepsilon$  equations. Assumption of zero boundary condition for  $\kappa$ ,  $\varepsilon$  equations on the rotor causes the laminar flow computations with zero values of  $\kappa$ ,  $\varepsilon$  in the whole computational region.

### Geometry and grid distribution

A schematic diagram of the geometry modelled is shown in Fig. 1. It is based on the experimental rotor-stator system used in measurement by PONCET *et al.* [18]. The system consists of a rotating disc (rotor) and a stationary disc (stator). A fixed shroud surrounds the system.

The outer and inner radii of the rotor are  $R_3 = 250$  mm and  $R_1 = 38$  mm, respectively. The outer radius of the system is  $R_2 = 253$  mm. There is a 3 mm radial gap between the rotating disc and the shroud. The inner radius of the stator is  $R_4 = 55$  mm. This makes a radial distance of 17 mm between the inner radius of the rotor and stator. This radial distance is used as an outlet port. There is an axial gap of  $h$  between the rotor and stator. In this study, 6 and 12 mm have been assigned to  $h$  as in the experimental setup.

In order to satisfy the low-Reynolds  $\kappa - \varepsilon$  model requirements ( $y^+ \leq 0.5$ ), a large number of grid points was packed near the wall and to model the inlet and outlet, fine grid used in these area and tried to keep the expansion/contraction parameter lower than 1.2. The grid distribution tests showed that a  $70 \times 140$

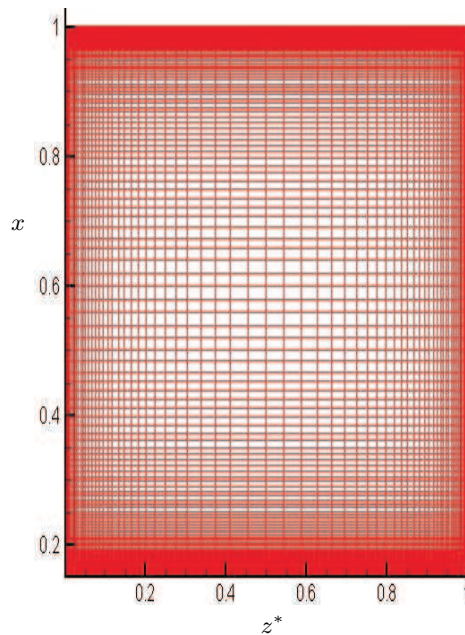


FIG. 2.  $70 \times 140$  (axial  $\times$  radial) computation grid with expansion factor 1.1.

(axial  $\times$  radial) was required. The mesh is illustrated in Fig. 2. In this figure,  $z^* = z/h$  and  $x = r/R_2$  are non-dimensional axial and radial coordinates, respectively.

#### Range of flow parameters

According to OWEN and ROGERS [15], the most effective dimensionless parameters that control the flow inside a rotor-stator system are the non-dimensional mass flow rate,  $C_w$ , and the rotational Reynolds number,  $Re_\varphi$ . The computed cases have been arranged in groups for which  $C_w$  varies while  $Re_\varphi$  and  $G$  remains constant and vice versa.

## 4. Results and discussion

#### Computed flow structure

Figures 3a and 3b show the computed streamline in the system for  $C_w = 5159$ ,  $G = 0.036$  and different values of  $Re_\varphi$ . Referring to these figures, it can be seen that flow structure mainly consist of three recirculation zones and a rotating core. The upper and lower recirculation zone are formed near the upper and lower shrouds. A rotating core fills most of the system. A stagnation point can be also distinguished. Here the stagnation point assumes the place where the radial velocity near the rotor changes its direction. The flow structure also consists of

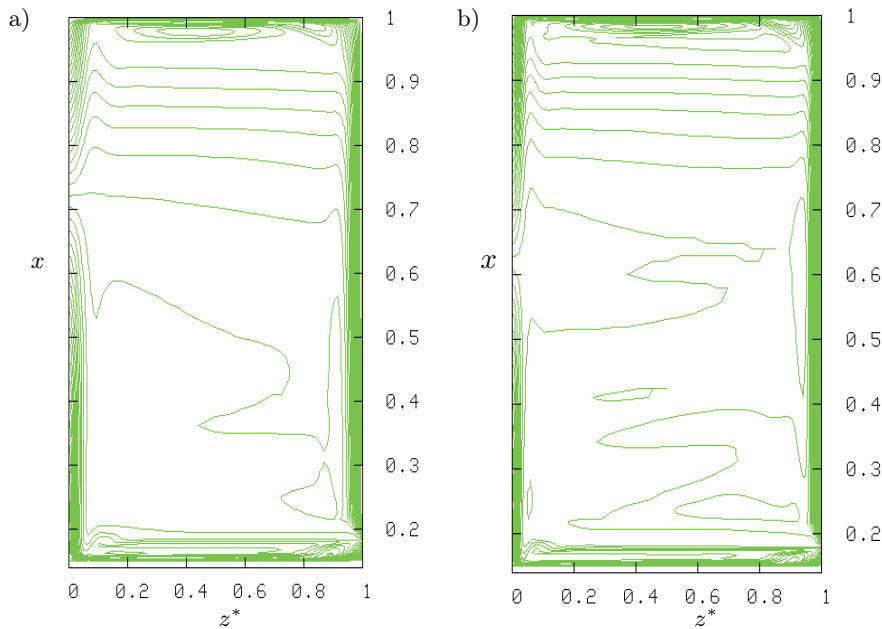


FIG. 3. Stream lines for  $C_w = 5159$ ,  $G = 0.036$  and a)  $\text{Re}_\varphi = 1.038 \times 10^6$ ,  
b)  $\text{Re}_\varphi = 2.076 \times 10^6$ .

two boundary layers on the rotor and the stator. It can be realized that the throughout inlet flow separated in two parts near the stagnation point. One part flows downwards through rotating boundary layer (Ekman layer) and then passes near the inner shroud and finally appears at the outlet. The most of other part flows upwards through the rotating boundary layer and then passes near the outer shroud and finally flows downwards through the stationary boundary and exits through the outlet.

#### Axial variation of dimensionless tangential velocity ( $V_\phi/\Omega r$ )

Figures 4 and 5 illustrate axial profiles of the dimensionless tangential velocity  $\beta = V_\phi/\Omega r$  and comparison with experimental data for  $\beta = 0.44, 0.68$  respectively. The effects of  $\text{Re}_\varphi$  and the radial position on the profiles could also be examined. Here the aspect ratio and non-dimensional flow rate ( $C_w = 10317$ ,  $G = 0.036$ ) are kept constant. In each case, the existence of the three characteristic zones: the two boundary layers and the rotating core, is exhibited. For  $x = 0.44$ ,  $\beta$  is greater than one in the core for the case where  $\text{Re}_\varphi = 1.038e6$ . This means that the fluid rotates faster than the disc in the core and consequently, as mentioned by OWEN and ROGERS [15], the direction of the flow in the boundary layer (here the Ekman layer) is radially inward. For the other cases  $\beta_\infty < 1$ , the direction of the flow in the boundary is radially outward. The direction of the flow in the

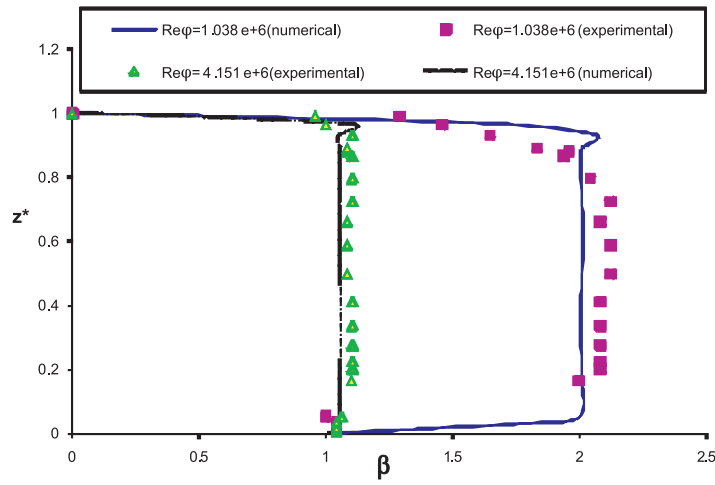


FIG. 4. Effects of the rotational Reynolds number on the axial profiles of the dimensionless tangential velocity for  $G = 0.048$ ,  $C_w = 5159$  and  $x = 0.44$  (experimental values provided by of PONCET *et al.* [18]).

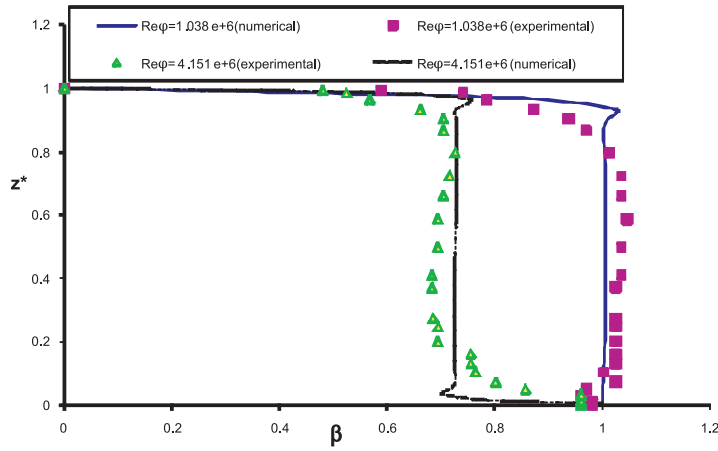


FIG. 5. Effects of the rotational Reynolds number on the axial profiles of the dimensionless tangential velocity for  $G = 0.048$ ,  $C_w = 5159$  and  $x = 0.68$  (experimental values provided by of PONCET *et al.* [18]).

boundary layers could be examined in Figs. 7 and 8. As discussed in more details by OWEN and ROGERS [15] for a sealed system (with no inlet or outlet flow), the structure of the flow is divided into three zones: a centrifugal boundary layer on the rotating disc, and a centripetal boundary layer on the stationary disc, divided by a rotating core where the tangential velocity doesn't vary and the radial component is nearly zero. By superimposing a centripetal throughflow,

the tangential velocity in the core increases. For a stronger centripetal flow, the two boundary layers are both centripetal what causes that the core rotates faster than the rotor. Referring to the Figs. 4 and 5, it can be seen that there is a good agreement between the computed and measured values.

#### Radial variation of dimensionless tangential velocity ( $V_\phi/\Omega r$ )

Figure 6 shows radial variation of the dimensionless tangential velocity  $\beta = V_\phi/\Omega r$  for  $z^* = 0.44$  which represents the core rotation. The effects of  $Re_\phi$  and the axial position could also be examined. Here the aspect ratio and non-dimensional flow rate ( $C_w = 10317$ ,  $G = 0.036$ ) are kept constant. It can be seen that the entrainment coefficient  $\beta$  is nearly constant for  $x > 0.4$  and is greater than 1 for lower values of  $Re_\phi$ . The entrainment coefficient is greater than 1 for lower value of  $x$ , which is due to the effects of rotating inner shroud and the outlet. The value of the entrainment coefficient is the lowest at  $x \approx 0.5$  when the effects of inner and outer shrouds as well as of the outlet are the smallest.

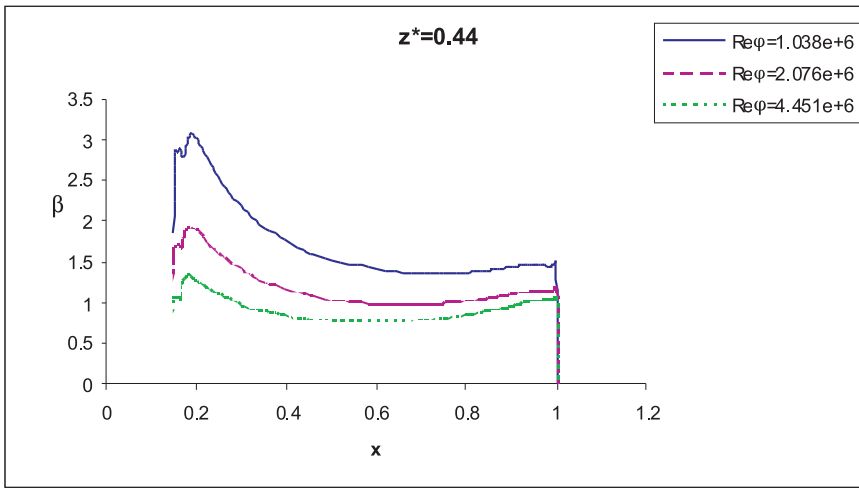


FIG. 6. Effects of the rotational Reynolds number on the radial variation of the dimensionless tangential velocity for  $G = 0.048$ ,  $C_w = 5159$ ,  $z^* = 0.44$ .

#### Axial variation of dimensionless radial velocity ( $v_r^* = V_r/\Omega r$ )

Effects of rotational Reynolds number on axial variation of radial velocity has been shown in Figs. 7 and 8 for  $x = 0.44$  and  $x = 0.68$  respectively. It is obvious that two boundary layers are formed near the rotor and stator. The boundary layer which is formed near the rotor is commonly referred to as Ekman-type and the one near the stator is called the Bödewadt layer. The radial velocity is zero

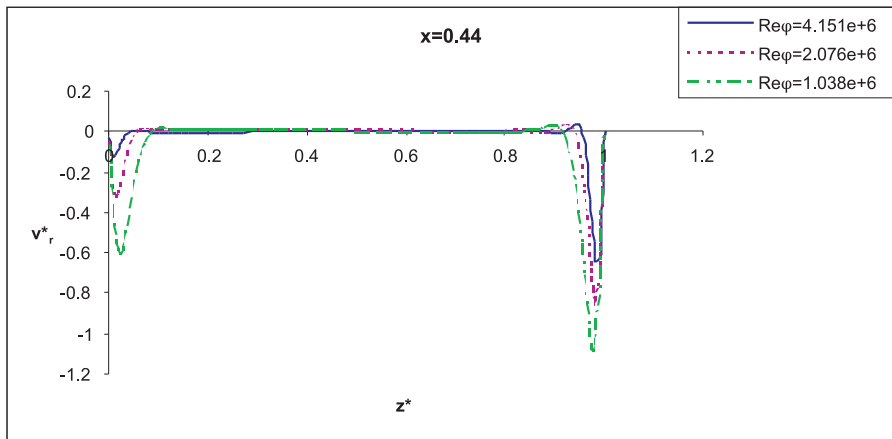


FIG. 7. Effects of the rotational Reynolds number on the axial profiles of the dimensionless radial velocity for  $G = 0.048$ ,  $C_w = 5159$  and  $x = 0.44$ .

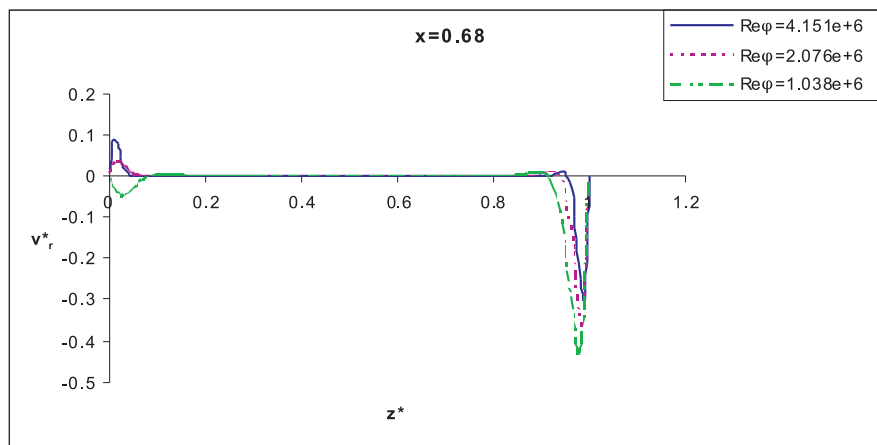


FIG. 8. Effects of the rotational Reynolds number on the axial profiles of the dimensionless radial velocity for  $G = 0.048$ ,  $C_w = 5159$ ,  $x = 0.68$ .

outside the boundary layers. This zone is commonly called the core. For a flow in rotating cavities in which rotational effects dominate, it is shown by OWEN and ROGERS [15] that  $V_r < 0$  in the boundary layer when  $\beta_\infty > 1$  and  $V_r > 0$  when  $\beta_\infty < 1$ . Referring to these figures, the same behaviour is encountered. As it can be seen when the Reynolds number increases, the radial velocity decreases and for the case  $x = 0.68$ , the direction of radial velocity on the rotor has been changed for the lowest Reynolds number. The position where the direction of radial velocity changes, is commonly called the stagnation point.

### Effect of flow parameters on the entrainment coefficient $\beta$

The effects of the rotational Reynolds number and the dimensionless flow rate,  $C_w$ , on the entrainment coefficient and comparison with the measured values are presented in Fig. 9 for  $G = 0.036$ . For  $C_w = 5159$  and a given radius  $x = 0.68$ , the dimensionless tangential velocity in the core,  $\beta$ , decreases for increasing values of  $Re_\varphi$ . This is due to the influence of stationary disc on the core which increases for higher value of  $Re_\varphi$ . On the other hand, in Fig. 10 where  $Re_\varphi = 1.038 \times 10^6$ , at  $x = 0.56$ ,  $\beta$  increases as  $C_w$  increases. As  $C_w$  increases,

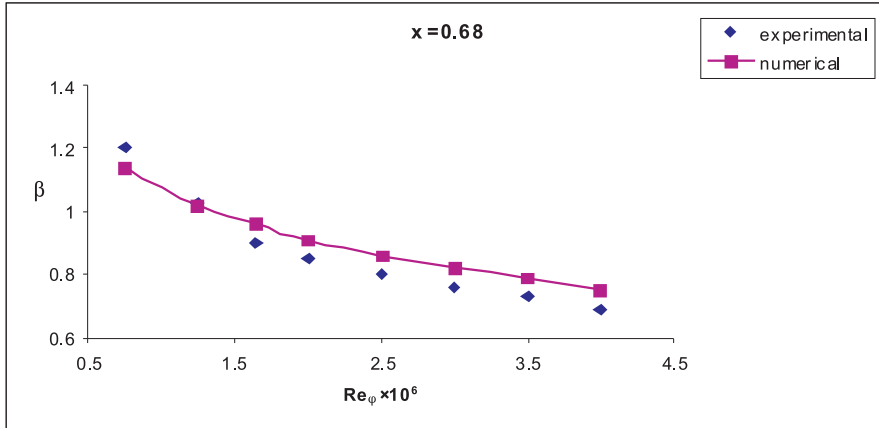


FIG. 9. Variation of  $\beta$  with  $Re_\varphi$ , for  $G = 0.036$ ,  $C_w = 5159$ ,  $z^* = 0.5$  and  $x = 0.68$  (experimental values provided by PONCET *et al.* [18]).

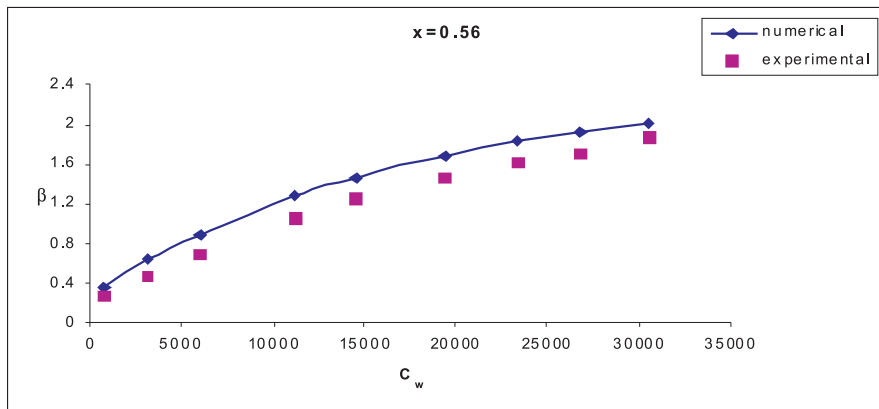


FIG. 10. Variation of  $\beta$  with  $C_w$ , for  $G = 0.036$ ,  $Re_\varphi = 1.038 \times 10^6$ ,  $z^* = 0.5$  and  $x = 0.56$  (experimental values provided by PONCET *et al.* [18]).

the amount of flow with  $\beta = 1$  which entered through the rotating disc also increases. This higher rotating flow raises the core rotation. The results have a fair agreement with experimental data. The effect of variation of the aspect ratio,  $G$ , on the entrainment coefficient  $\beta$  has been compared in Fig. 11 when  $G$  varies between 0.024, 0.036 and 0.048 and for  $\text{Re}_\phi = 4.151 \times 10^6$  and  $C_w = 5159$ . It is clear that  $\beta$  is not sensitive to the variations of  $G$ , as the flows remain in the same regime (turbulent with separated boundary layers).

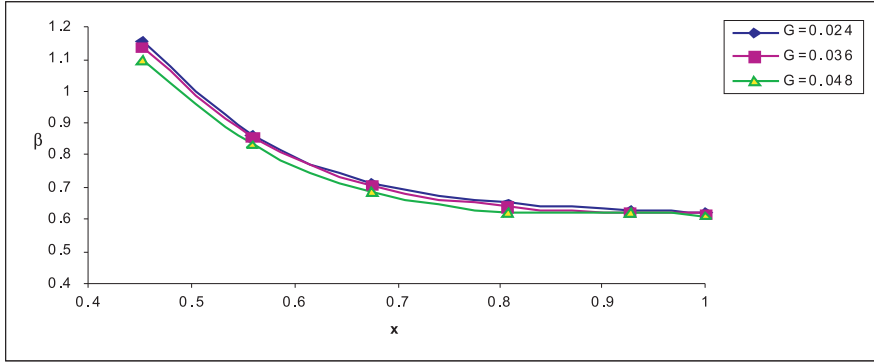


FIG. 11. Effects of aspect ratio,  $G$ , on the entrainment coefficient  $\beta$  for  $\text{Re}_\phi = 4.151 \times 10^6$ ,  $z^* = 0.5$  and  $C_w = 5159$ .

#### Effect of rotational Reynolds number on moment coefficient $C_m$

The moment coefficient,  $C_m$ , for inner side of the rotating disc is defined as:

$$(4.1) \quad C_m = -2\pi \int_0^b r^2 \tau_{\phi,w} dr / \frac{1}{2} \rho \Omega^2 R_2^5,$$

where  $\tau_{\phi,w}$  is the shear stress on the rotating disc. As  $y^+ < 1$ , the first grid point is always inside the viscous sublayer, hence:

$$(4.2) \quad \tau_{\phi,w} = \mu \left. \frac{\partial V_\phi}{\partial z} \right|_{z=0}.$$

The influence of rotational Reynolds number and the dimensionless flow rate  $C_w$  on the moment coefficients which have been computed for the rotating disc using Eq. (4.1), are shown in Figs. 12 and 13 respectively. It is obvious that moment coefficient,  $C_m$ , decreases for increasing values of  $\text{Re}_\phi$ . This is due to thickening of the boundary layer thickness on the rotor which could be seen in

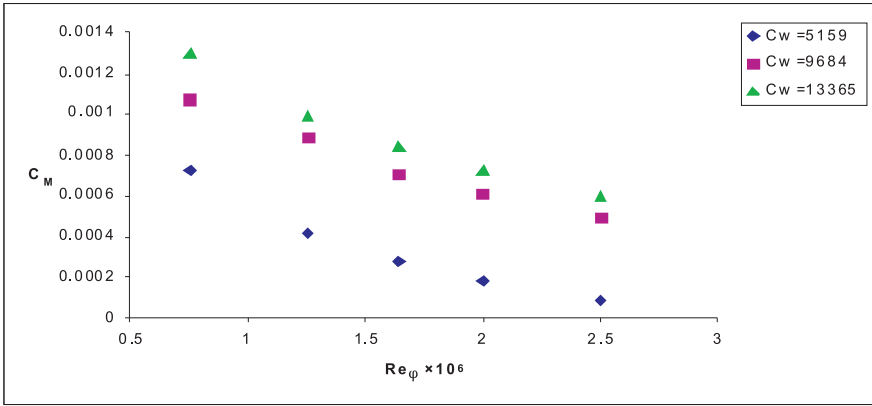


FIG. 12. The effect of  $Re_\varphi$  on moment coefficient  $C_m$  for  $G = 0.036$ .

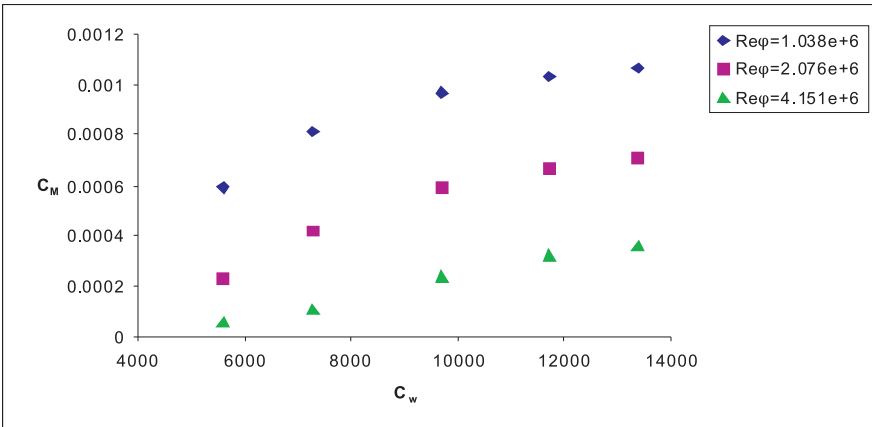


FIG. 13. The effect of  $C_w$  on moment coefficient  $C_m$  for  $G = 0.036$ .

Figs. 7 and 8. On the other hand,  $C_m$  increases as  $C_w$  increases. Considering Fig. 15, it can be realized that for constant  $C_w$ , there is a critical value of  $Re_\varphi$  in which  $C_m = 0$ .

By combining the effects of  $Re_\varphi$  and  $C_w$  and the definition of turbulent flow parameters ( $\lambda_T = C_w / Re_\varphi^{0.8}$ ), a formula for estimating  $C_m$  in the system is presented below:

$$(4.3) \quad C_m = 0.0006 \ln(\lambda_T) + 0.002.$$

Figure 14 shows numerical values of  $C_m$  against the turbulent flow parameters, along with the correlated values of Eq. (4.2). Note from the figure that  $\lambda_T$  increases when  $C_m$  increases. At  $\lambda_T \cong 0.03$ ,  $C_m$  approaches zero which indicates

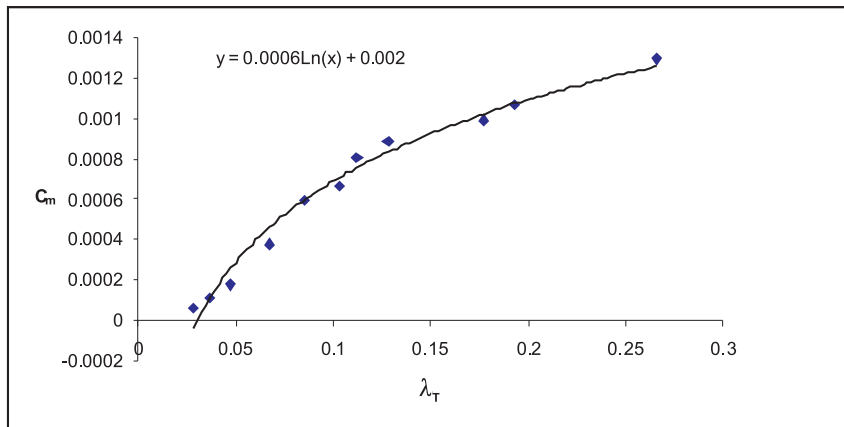


FIG. 14. The variation of moment coefficient with  $\lambda_T$  for  $G = 0.036$ .

a critical point. The critical point (where  $C_m$  approaches zero) is a significant result for the designer since the amount of the external work is minimum at this point. It is interesting to note that KARABAY *et al.* [8] and FARZANEH [3] have also found a critical value for another flow parameter (inlet swirl ratio) in which  $C_m$  approaches zero for other configuration.

**Estimation of the stagnation point**

The stagnation point,  $x^*$ , on the rotor is the point where the direction of radial velocity in the Ekman layer is changed. Basing on the numerical computation, the stagnation points for various cases have been calculated. Figure 15 shows variation of  $x^*$  against  $Re_\varphi$ . A fitted curve is also presented in the figure.

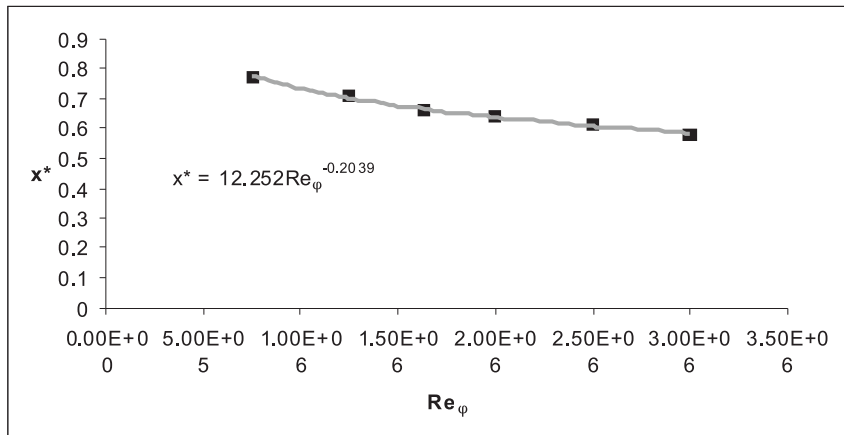


FIG. 15. The variation of stagnation point against  $Re_\varphi$ .

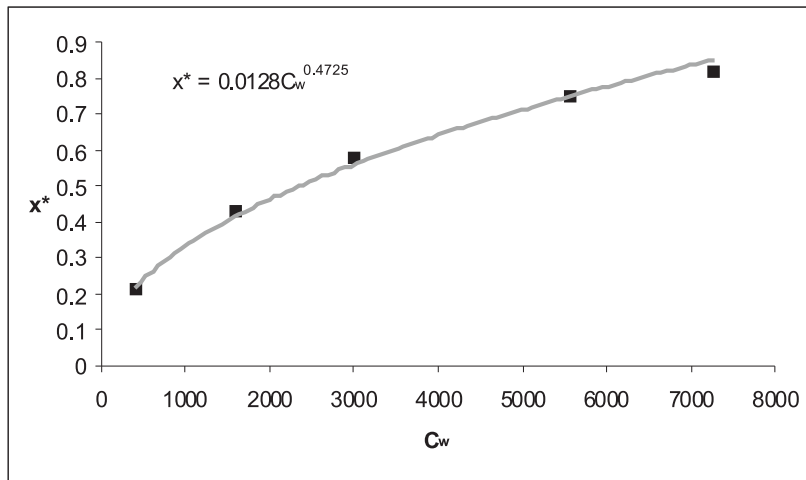


FIG. 16. The variation of stagnation point against  $C_w$ .

It is obvious that  $x^*$  decreases as  $\text{Re}_\varphi$  increases. Figure 16 shows variation of  $x^*$  against  $C_w$ . It can be seen that  $x^*$  increases when  $C_w$  increases.

By combining effects of  $\text{Re}_\varphi$  and  $C_w$  and the definition of turbulent flow parameters as  $\lambda_T = C_w/\text{Re}_\varphi^{0.8}$ , a formula for estimating the position of stagnation point in the system is presented below:

$$(4.4) \quad x^* = 0.2131 \text{Ln}(\lambda_T) + 1.2876.$$

Figure 17 shows numerical values of the stagnation point against the turbulent flow parameters, along with the correlated formula values of Eq. (4.2). Note

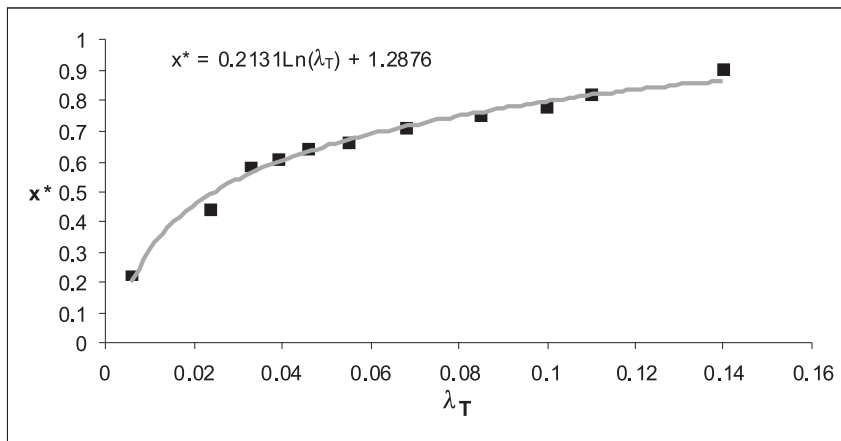


FIG. 17. The variation of stagnation point against  $\lambda_T$

from the figure, that as  $\lambda_T$  increases, the stagnation point moves towards the outer shroud.

## 5. Conclusions

A computational study has been carried out to investigate the turbulent flow inside a rotor–stator system and to examine the effects of flow parameters (rotational Reynolds number, non-dimensional flow rate and aspect ratio) on the flow structure. The available measured values have been also compared with the numerical values.

The contours of streamlines and axial variation of velocity profile show that there are two separated boundary layers on each disc with a rotational core in the middle, which is commonly found in a classical rotor-stator system. For lower value of non-dimensional flow rate, the flow structure is similar to a sealed system. In the case of a higher centripetal throughflow, the flow is then divided into three areas in which the central core rotates faster than the rotating disc and both boundary layers are centripetal.

The results show that there is a stagnation point on the boundary layer formed near the rotating disc (commonly known as the Ekman layer). The stagnation point moves towards the shroud when rotational Reynolds number decreases or non-dimensional flow rate increases. A correlation has been given to estimate the position of the stagnation point. The computed values of the momentum coefficient decrease for increasing values of rotational Reynolds number or for decreasing non-dimensional flow rate. The computed results show that there is a critical value for flow parameters, in which the momentum coefficient approaches zero.

The computed values are in good agreement with the measured values what has proved that the computation method can be used as a reasonable tool to investigate the flow inside the rotor-stator system.

## References

1. G.K. BATCHELOR, *Note on a class of solutions of Navier–Stokes equations representing steady rotationally-symmetric flow*, Q. J. Mech. Appl. Maths, **4**, 29–41, 1951.
2. J.W. DAILY, R.E. NECE, *Chamber dimension effects on induced flow and frictional resistance of enclosed rotating discs*, Trans. ASME: J. Basic Eng., **82**, 217–232, 1960.
3. M. FARZANEH-GORD, *Flow and heat transfer in a pre-swirl rotor-stator system*, PhD thesis, University of Bath, 2003.
4. M. FARZANEH-GORD, *Axisymmetric study of flow in pre-swirl rotor-stator system*, 14th annual (international) conferences on Mechanical Engineering, 16–18 May 2006, ISME2006.
5. M. FARZANEH-GORD, *Heat transfer over rotor surface in a pre-swirl rotating-disc system*, International Journal of Dynamics of Fluids, (IJDF), **3**, No. 1, June 2007.

6. A.D. GOSMAN, F.J.K. IFERIAH, *Tech-T: A general computer program for two-dimensional turbulent recirculating flows in calculations of recirculating flows*, Mech. Eng. Dept., Imperial College, Univ. of London, 1976.
7. D. GROHNE, *Über die laminare Strömung in einer kreiszylindrischen, Dose mit rotierendem Deckel*, Nachr. Akad. Wiss. Göttingen, Math. Phys. Kl., 263-282, 1955.
8. H. KARABAY, M. WILSON, J.M. OWEN, *Predictions of effect of swirl on flow and heat transfer in a rotating cavity*, Int. J. Heat Fluid Flow, **22**, 143-155, 2001.
9. B.E. LAUDER, B.L. SHARMA, *Applications of the energy dissipation model of turbulence to the calculation of flow near a spinning disc*, Letters in Heat and Mass Transfer, **1**, 131-138, 1974.
10. G.N. LANCE, M.H. ROGERS, *The axially symmetric flow of a viscous fluid between two infinite rotating discs*, Proc. Roy. Soc., A, **266**, 109-121, 1962.
11. P.R. LEWIS, M. WILSON, G.D. LOCK, J.M. OWEN, *Effect of radial location of nozzles on performance of preswirl systems: a computational and theoretical study*, Proc. Institution of Mechanical Engineers, Part A: Journal of Power and Energy, **223**, No. 2, 179-190, ISSN 0957-6509, 2009.
12. P.R. LEWIS, M. WILSON, G.D. LOCK, J.M. OWEN, *Physical interpretation of flow and heat transfer in pre-swirl systems*, J. Engineering for Gas Turbines and Power, **129**, 3, 769-777, 2007, ISSN 00742-4795.
13. G.D. LOCK, Y. YAN, P.J. NEWTON, M. WILSON, J.M. OWEN, *Heat transfer measurements using liquid crystals in a pre-swirl rotating-disc system*, J. Engineering for Gas Turbines and Power, **127**, 2, 375-382, ISSN 0742-4795, 2005.
14. M. NALLASAMY, *Turbulence models and their applications to the prediction of internal flows: a review*, Computers & Fluids, **15**, 151-194, 1987.
15. J.M. OWEN, R.H. ROGERS, *Flow and heat transfer in rotating disc systems: Vol. 1, Rotor-stator systems*, Research Studies Press, Taunton, UK and John Wiley, NY, 1989.
16. C.E. PEARSON, *Numerical solutions for the time-dependent viscous flow between two rotating coaxial discs*. J. Fluid Mech., **21**, 623-633, 1965.
17. K.G. PICHA, E.R.G. ECKERT, *Study of the air flow between coaxial discs rotating with arbitrary velocities in an open or enclosed space*, Proc. 3rd U. S. Nat. Cong. Appl. Mech., 791-798, 1958.
18. S. PONCET, M.P. CHAUVE, P. LEGAL, *Turbulent rotating disc flow with inward through-flow*, J. Fluid Mech., **522**, 253-262, 2005.
19. K. STEWARTSON, *On the flow between two rotating coaxial discs*, Proc. Camb. Phil. Soc., **49**, 333-341, 1953.
20. M. WILSON, J.X. CHEN, J.M. OWEN, *Computation of flow and heat transfer in rotating-disc systems*, Trans. IMechE 3<sup>rd</sup> Int. Conf. on Computers in Reciprocating Engines and Gas Turbines, pp. 41-49, 1996, ISBN 0 85298 084 9-A.

Received July 1, 2009; revised version February 4, 2010.

---